ARTICLE

In-situ Synthesis of Silver Chloride Nanoparticle-Loaded Attapulgite Composites with Efficient Antimicrobial Activity

Zhang Kefeng[1,2], Li Yan[1,2], Nie Kailong[1,2], Dang Shiyuan[1,2], Yao Bingxue[1], Hua Xue[1,2], Tian Guangyan[1,2]

[1] School of Materials Science and Engineering, Hebei University of Technology, Tianjin 300130, China; [2] Key Laboratory of Special Functional Materials for Ecological Environment and Information, Ministry of Education, Hebei University of Technology, Tianjin 300130, China

Abstract: To enhance the dispersibility and photostability of AgCl nanoparticles (NPs), AgCl NPs were firmly anchored on the surface of attapulgite (ATP) to prepare the ATP-AgCl composites. The microstructure, crystal structure, and antibacterial activity of the ATP-AgCl composites were investigated. Results demonstrate that the introducion of ATP not only avoids the agglomeration of AgCl NPs, but also decreases their particle size from $5-10$ μm to $3-20$ nm. Due to the small size effect of NPs, the antibacterial activity of as-prepared ATP-AgCl composites is comparable to that of pure AgCl. The antibacterial ratios against Escherichia coli and Staphylococcus aureus are 99.98% and 99.88%, respectively. Additionally, the introduction of ATP also improves the photostability of AgCl NPs: the composites remains offwhite after exposure to sunshine for 24 h.

Key words: attapulgite; silver chloride; inorganic antibacterial agent; Escherichia coli; Staphylococcus aureus

Inorganic antibacterial agents attract much attention because of their broad spectrum, high efficiency, and environmental-friendly advantages[1]. Among them, AgCl nanoparticles (NPs) attract considerable attention due to their strong antibacterial activity and broad antibacterial spectra[2]. AgCl NPs can break the cell wall of bacteria and hinder the electron transfer between the cytochrome system and DNA synthesis, leading to the production of reactive oxygen species[3–4]. Due to their multi-target antimicrobial mechanism, bacteria hardly have resistance against AgCl NPs. However, AgCl NPs are prone to agglomeration, which increases their size and decreases the antibacterial activity[5–6]. AgCl NPs exhibit inferior photostability: they turn purple and then gradually darken under light exposure[7], which discolors the product and reduces their commercial value. Besides, AgCl NPs are expensive. These problems all restrict the application of AgCl NPs in the antimicrobial field. Hence, the development of AgCl antibacterial agents with strong antibacterial properties, good dispersion, photostability, and low cost is crucial and urgent.

To solve the abovementioned problems, various strategies and in-depth studies have been proposed and investigated. Fanoro et al[8] prepared Ag-Au bimetallic material as antibacterial NP, which is superior to single metal NP due to the synergistic effect between metals. Al-Tayyar et al[9] synthesized bio-composite membranes consisting of SiO_2 NPs doped with ZnO NPs, which exhibit excellent antibacterial activity. Mei[10] and Mohapatra[11] et al introduced graphene oxide (GO) to establish the GO-Ag nanosystem, which synergistically enhances the antibacterial activity against Escherichia coli (E. coli) and Staphylococcus aureus (S. aureus), compared with that of pure Ag NPs. Therefore, the preparation of AgCl composite antimicrobial agents is expected to improve the antimicrobial activity of AgCl NPs.

Attapulgite (ATP) is a natural water-containing silicate mineral with layer-chain transition structure, whose stoichiometric composition is $Si_8Mg_5O_{20}(OH)_2(OH_2)_4 \cdot 4H_2O$, belonging to the sepiolite family in mineralogy[12]. As a natural nanomaterial, ATP is an excellent carrier material because of its unique rod morphology and pore structure[13–14]. Shi et al[15] studied the removal process of nitrogen from low-carbon source sewage by the membrane bioreactor-ATP integrated

system. Li et al[16] synthesized the fluoride-ATP NPs by microwave hydrothermal method for photocatalytic nitrogen fixation. Zhang et al[17] evaluated the potential of ATP as nickel catalyst carrier in hydrogen production from acetic acid steam reforming. China is extremely rich in ATP resource[18], which accounts for about 60% of the global reserve. ATP as carrier material cannot only reduce the cost but also achieve the purpose of safety, environment protection, and energy saving, which has broad application prospects in the development of AgCl antibacterial agent.

Herein, a series of ATP-AgCl composites were prepared by simple and feasible strategy with ATP as carrier. The schematic diagram of synthetic process of ATP-AgCl composites is shown in Fig. 1. The microstructure, crystal structure, and antibacterial activity of the composites were characterized. This research is beneficial to the development of highly efficient inorganic antimicrobial agents and the high value-added utilization of natural minerals.

1 Experiment

ATP was provided by Gansu Rongwan Technology Co., Ltd. CH_3COOAg (AR) was supplied by Tianjin Dongjulong Chemical Technology Development Co., Ltd. NH_4Cl and $NH_3 \cdot H_2O$ (AR) were provided by Tianjin Fengchuan Chemical Reagent Technology Co., Ltd. Agar powder (No. A505255-0250) and broth culture medium (No. A507002) were supplied by Bioengineering Co., Ltd. The strains used in the experiment were E. coli (No. ATCC 25922) and S. aureus (No. ATCC 29213).

ATP-AgCl composites were prepared by a simple hydrothermal process. ATP (1.0 g) was dissolved in 60.0 mL deionized water and ultrasonically stirred for 10 min. NH_4Cl (0.5 g) and CH_3COOAg of different masses were mixed and stirred to form homogeneous solution consisting of 1wt%, 2.5wt%, 5wt%, 7.5wt%, and 10wt% AgCl. Then, 2.0 mL $NH_3 \cdot H_2O$ was added into the mixed solution drop by drop. Afterwards, the solution was ultrasonically stirred and transferred to the 100.0 mL Teflon lined autoclave, which was sealed and maintained at 140 °C for 12 h. Finally, the white product was collected after the autoclave was cooled to room temperature. Then, the product was washed several times by deionized water. The final products were marked as ATP-1AgCl, ATP-2.5AgCl, ATP-5AgCl, ATP-7.5AgCl, and ATP-10AgCl composites, according to the mixed solution containing 1wt%, 2.5wt%, 5wt%, 7.5wt%, and 10wt% AgCl, respectively.

LB liquid culture medium: 100.0 mL of deionized water
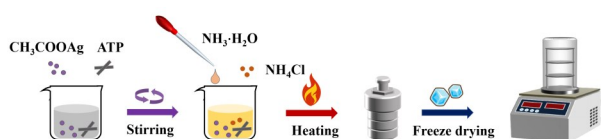
Fig.1 Schematic diagram of synthetic process of ATP-AgCl composites

and 2.5 g LB broth culture medium were placed in a 250.0 mL reagent bottle, mixed evenly, and then sterilized in a high-temperature and high-pressure steam sterilization pot at 121 °C for 15 min.

Preparation of LB solid culture medium was as follows. The deionized water (100.0 mL), LB broth culture medium (2.5 g), and agar powder (1.5 g) were placed in 250.0 mL reagent bottle, mixed evenly, and then sterilized in a high-temperature and high-pressure steam sterilization pot at 121 °C for 15 min. After the medium was cooled to 40–50 °C, 15.0 mL medium was absorbed by the electric pipette and poured into a disposable sterile plate.

LB liquid medium (3.0 mL) and single colony selected from the solid medium of E. coli and S. aureus strains were added into the bacterial culture tubes of 12.0 mL, separately. The third bacterial culture tube had no additives, and it was used as blank control. These culture tubes were placed in the thermostatic oscillator (37 °C, 200 r/min) and incubated for 15 h. The concentration of bacterial solution was adjusted to 10^8 CFU/mL by comparison with the bacterial turbidimeter.

The sample (0.08 g) was weighed and placed in a centrifuge tube, then autoclaved at 121 °C for 20 min, and dried for standby. The circular filter paper with diameter of 1 cm was placed in the centrifuge tube, then autoclaved at 121 °C for 20 min, and dried for standby. The sample suspensions of 40 mg/mL were prepared by adding 2.0 mL sterile pure water to the powder sample. Then, the sterilized filter paper was put into the sample suspensions and soaked overnight for standby. The concentrations of E. coli and S. aureus were diluted to 10^6 CFU/mL by sterile phosphate buffer saline (PBS) solution, separately. The diluent (100.0 µL) was evenly coated on the LB solid culture medium. Then, according to the grouping, the filter paper pieces soaked in the sample suspension overnight were pasted on the surface of the culture medium with sterile tweezers, and they were gently pressed for complete contact between the sample and culture medium. Finally, the Petri dish was incubated in the constant temperature incubator at 37 °C for 24 h. The diameter of bacteriostatic circle was measured by vernier caliper.

Sterile pure water (2.0 mL) was added into the sterilized sample. After sufficient mixture, the sample suspension of 20 mg/mL was obtained. The concentration of E. coli broth was diluted to 10^6 CFU/mL in LB liquid medium. The diluted bacterial solution (1.8 mL) was added to the bacterial culture tube, and then 200.0 µL sample suspension was added according to the grouping (in this case, the working concentration of the sample was 2 mg/mL). The sterile pure water (200.0 µL) was added into the blank control group. The bacterial culture tube was placed in a thermostatic oscillator at 37 °C and incubated at 200 r/min for 6 h. After the culture was completed, the bacterial solution was continuously diluted by 10 times using the sterile PBS solution with dilution ratio of 10^4 set. Then, the dilution (100.0 µL) was uniformly coated on the LB solid culture medium. Finally, it was placed in the constant temperature incubator at 37 °C for 18 h. Afterwards, the sample was observed and the bacterial

colonies were recorded.

The bacterial liquid concentration (CFU/mL) with 0.1 mL coated dilution and the bacteriostatic ratio can be calculated by Eq.(1) and Eq.(2), respectively, as follows:

$$\text{Bacterial liquid concentration}=\text{Colony count}\times\text{Dilution ratio}\times 10 \tag{1}$$

$$\text{Bacteriostatic ratio} = (1 - \frac{\text{Bacterial liquid concentration in experiment group}}{\text{Bacterial liquid concentration in control group}}) \times 100\% \tag{2}$$

The morphologies and microstructures of the samples were characterized by field emission scanning electron microscope (SEM, NOVANanoSEM450, FEI, USA), transmission electron microscope (TEM, Tecnai G2 F20 S-TWIN, FEI, USA), high resolution TEM (HRTEM), energy dispersive spectroscope (EDS), and high angle annular dark field-scanning transmission electron microscope (HAADF-STEM). The phase composition of the samples was determined by X-ray diffractometer (XRD, Cu-Kα, D8 ADVANCE, Bruker, Germany) to assess possible structural changes. The pore size and specific surface area of the samples were determined by N_2 adsorption-desorption analyzer (BET, Cryosync, Autosorb IQ, USA), which was degassed at 250 °C for 12 h. The functional groups of the samples were analyzed by Fourier transform infrared spectroscopy (FTIR, VERTEX80, Bruker, Germany) using the potassium bromide particle technique.

2 Results and Discussion

2.1 Morphology and structure characterization

The morphologies and microstructures of the as-prepared AgCl, ATP, and ATP-10AgCl composite were observed by SEM and TEM, as shown in Fig. 2. AgCl NPs are smooth microspheres with particle size of 5 – 10 μm[19], and the particles are agglomerated[20], as shown in Fig. 2a. ATPs are short rods with smooth surface without loaded particles (Fig. 2b). Compared with AgCl NPs, the addition of ATP not only avoids the agglomeration of AgCl NPs, but also sharply reduces the particle size of AgCl NPs to 3–20 nm (Fig. 2e). Choi et al[21] reported that the size of AgCl colloidal antibacterial agent is 250 nm, whereas Mao et al[22] reported that the size of Ag@AgCl is about 600 nm. It can be seen that ATP can effectively control the growth of AgCl NPs. The small size of AgCl NPs provides a larger specific surface area, which promotes the NP adsorption on the bacterial surface and increases the chance of interactions between AgCl NPs and bacterial cell membranes[23]. It is known that AgCl NPs with size smaller than 10 nm can directly penetrate the cell membranes and interact with proteins and DNA, therefore causing cell damage[24]. The lattice stripe with length of 0.24 nm (Fig. 2f) belongs to the (200) crystallographic plane of AgCl, demonstrating that the black particles are AgCl NPs. HAADF-STEM images and EDS element mapping restuls show that Ag, Cl, Si, Mg, Al, and O atoms are uniformly distributed in ATP-10AgCl composite. The elements distributed at NPs are mainly Ag and Cl, which also confirms the successful synthesis of AgCl NPs.

Fig. 3 shows XRD patterns of different ATP-AgCl composites to analyze the phase composition of NPs. The M, W, and Q diffraction peaks denote the muscovite, whewellite, and quarte, respectively, which are the main components of ATP. Among them, XRD pattern of AgCl is consistent with the standard PDF card of AgCl (JCPDS file: 31-1238). According to XRD patterns of ATP-AgCl composites, the intensity of the characteristic diffraction peak of AgCl is increased with increasing the loading of AgCl. When the loading of AgCl is 1wt%, 2.5wt%, and 5wt%, only a trace amount of AgCl can be detected. When the loading of AgCl increases to 7.5wt% and 10wt%, the characteristic peaks of AgCl can be clearly observed. The diffraction peaks at 27.82°, 32.24°, 46.23°, 54.83°, 57.48°, and 67.47° correspond to the (111), (200), (220), (311), (222), (220), (311), and (222) crystallographic planes of AgCl (JCPDS file: 31-1238), respectively. Comparably, the peak intensity of AgCl in the ATP-AgCl composites is lower than that of pure AgCl. Meanwhile, the sharp, narrow, and high peaks change to stubby and dwarf ones, reflecting that the preparation of ATP-AgCl composites with ATP as carrier reduces the size of AgCl NPs[25]. XRD analysis results agree well with SEM and TEM analysis results.

FTIR spectra of AgCl, ATP-10AgCl composite, and ATP are shown in Fig. 4. The peaks with wavenumber greater than 3000 cm^{-1} mainly correspond to the hydroxyl groups of ATP surface, such as the stretching vibrations of adsorbed water and crystalline water. In the low and middle frequency regions, the peaks with wavenumber less than 1670 cm^{-1} mainly correspond to the bending vibrations of crystalline water inside ATP and the stretching vibrations of Si-O bond in silica-oxygen tetrahedral sheet. Compared with FTIR spectrum of ATP, the absorption peaks of ATP-10AgCl composite only change slightly in intensity and their positions do not change significantly, indicating that the loading of AgCl NPs on the ATP surface does not significantly affect the crystal structure of ATP.

The abovementioned results are further verified through N_2 adsorption-desorption isotherms. As shown in Fig. 5, the N_2 adsorption-desorption isotherm of ATP-10AgCl composite is a typical IV type isotherm. In the low pressure stage, the adsorption curve is relatively flat, indicating that the channels for the adsorption of N_2 molecules of ATP-10AgCl composite are monolayer. In the high pressure stage, the N_2 adsorption is increased rapidly with increasing the relative pressure. Under this condition, the adsorption channels of N_2 molecules change from monolayer to multilayer, which leads to the capillary coalescence phenomenon in the pores or channels. In the high pressure stage, H3 type hysteresis loops appear, which are usually found in the materials with medium or large pores produced by aggregation of laminar structure. These pores are characterized by not exhibiting adsorption saturation in the higher relative pressure region.

The specific surface area of ATP-10AgCl composite is very small of only 24.92 m$^2\cdot$g^{-1}, and the unit pore volume is
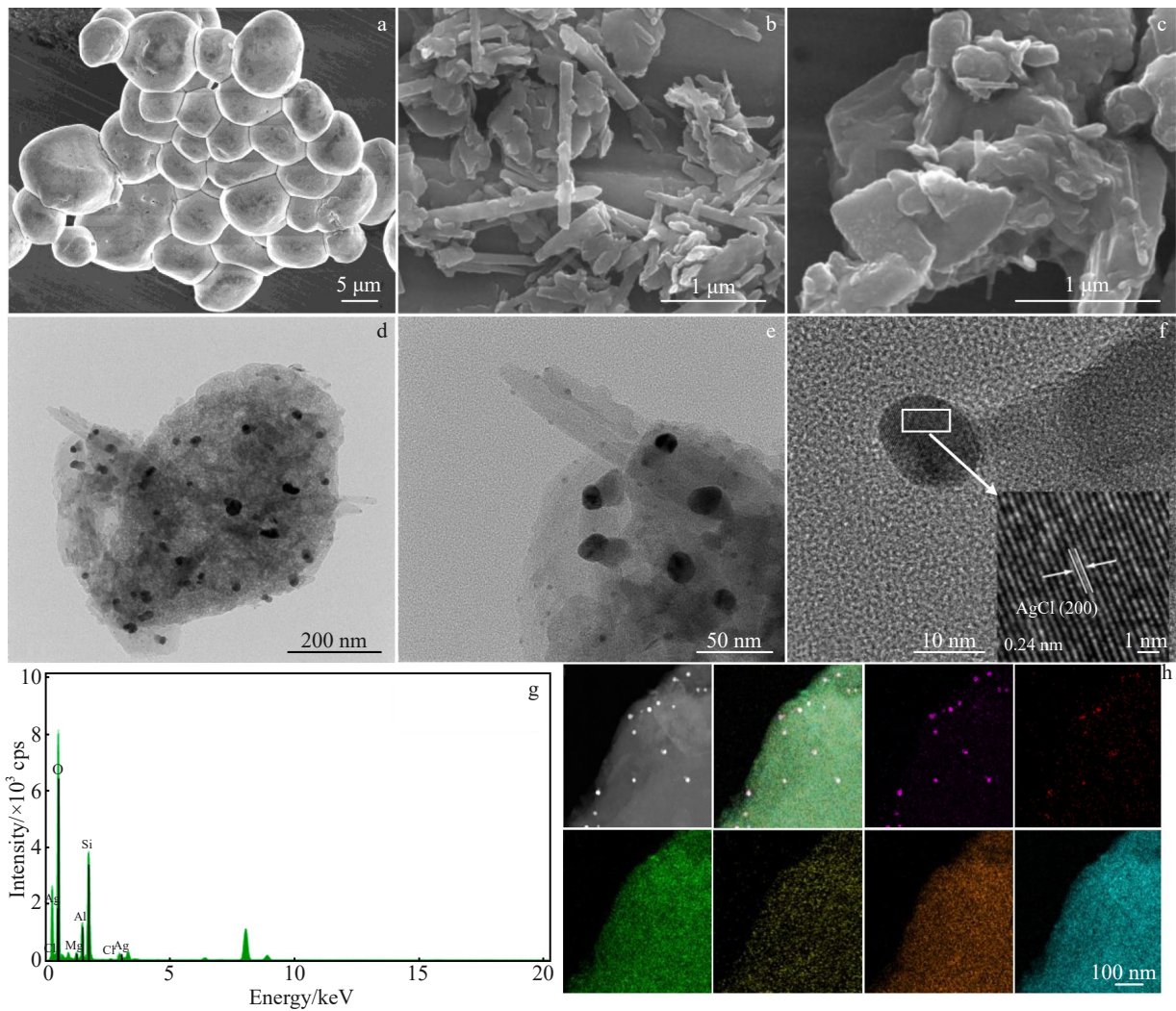
Fig.2   SEM morphologies of AgCl (a), ATP (b), and ATP-10AgCl composite (c); TEM images (d–e), HRTEM image (f), EDS spectrum (g), and HAADF-STEM images coupled with EDS element mapping results (h) of ATP-10AgCl composite
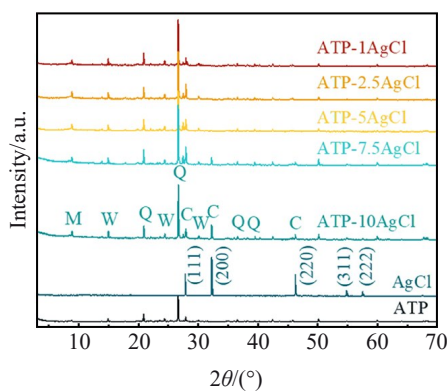
Fig.3   XRD patterns of different ATP-AgCl composites, AgCl, and ATP
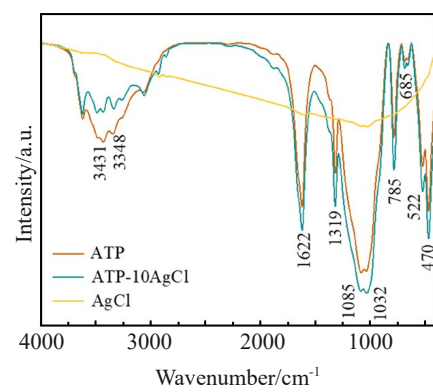
Fig.4   FTIR spectra of ATP, ATP-10AgCl composite, and AgCl

0.11 cm³·g⁻¹. Combined with Fig.2, it is inferred that the small specific surface area and unit pore volume are caused by the coverage of AgCl NPs on the ATP surface. According to the

pore size distribution of ATP-10AgCl com-posite, a broad peak appears at 21.15 – 31.42 nm (Fig. 5b). The pore size of ATP-10AgCl composite is concentrated at 21.15 – 31.42 nm, indicating that ATP-10AgCl composite belongs to the
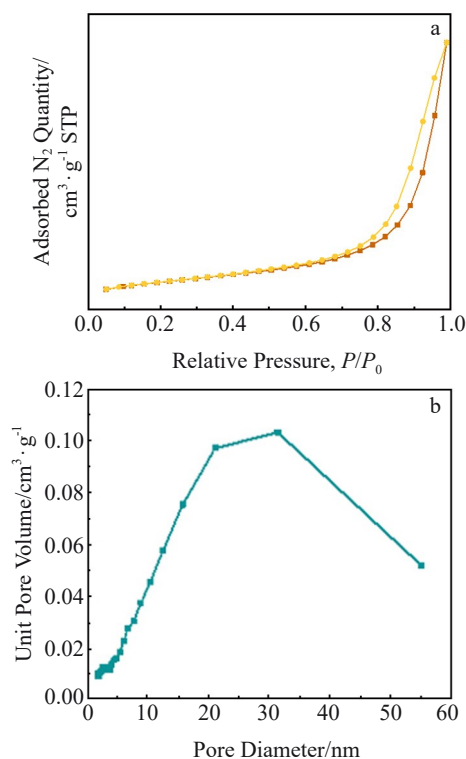
Fig.5 N$_2$ adsorption-desorption isotherms (a) and pore size distribution (b) of ATP-10AgCl composite

mesoporous material. Furthermore, the phenomenon corresponds to the IV type isotherm and H3 type hysteresis loop.

2.2 Antibacterial activity

The antibacterial activities of ATP-AgCl composites and pure AgCl were investigated with E. coli and S. aureus as the target bacteria. As shown in Fig. 6, the average diameters of the inhibition circles of ATP-1AgCl, ATP-2.5AgCl, ATP-5AgCl, ATP-7.5AgCl, ATP-10AgCl, and AgCl against E. coli are 2, 3, 6, 6, 6, and 6 mm, respectively. The average diameters of the inhibition circles of ATP-1AgCl, ATP-2.5AgCl, ATP-5AgCl, ATP-7.5AgCl, ATP-10AgCl, and AgCl against S. aureus are 2, 5, 7, 8, 8, and 9 mm, respectively. No inhibition circles appear in the control group. The antibacterial performance of ATP-AgCl composites is not continuously enhanced with increasing the loading of AgCl. When the loading of AgCl reaches 10wt%, ATP-10AgCl composite has comparable antibacterial effect as pure AgCl, which indicates that ATP can effectively reduce the consumption of AgCl,
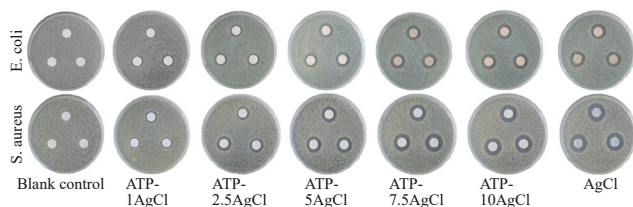
Fig.6 Inhibition circles of E. coil and S. aureus with different ATP-AgCl composites and AgCl

therefore decreasing the cost.

Furthermore, minimal inhibitory concentration (MIC) tests were conducted to investigate the antibacterial effect of the ATP-10AgCl composite against E. coli and S. aureus. As shown in Fig. 7 and Fig. 8, there are no bacterial colonies at dilution ratios of 10^5 with the presence of ATP-10AgCl composite. At dilution times of 10^4, no E. coli colonies can be observed, and the bacterial liquid concentration is lower than 1.0×10^5 CFU/mL. The antibacterial ratio of ATP-10AgCl composite against E. coli is larger than 99.98%. As for the antibacterial effect against S. aureus, the bacterial liquid concentration is 1.5×10^6 CFU/mL, and the bacteriostatic ratio is 99.88% (Fig. 8). Obviously, the antibacterial effect of ATP-10AgCl composite against E. coli is better than that against S. aureus. This is because the cell walls of Gram-negative strains (E. coli) are looser and have less layers than the Gram-positive bacteria (S. aureus) do, which is more conducive to the penetration of NPs[24,26]. In general, the small AgCl NPs are conductive to the enhancement in antibacterial performance, and ATP-10AgCl composite has excellent antibacterial properties.

2.3 Photostability analysis

With the synergistic effect of AgCl and ATP, the ATP-AgCl composites also have excellent photostability. As shown in Fig. 9, AgCl is extremely unstable, which easily decomposes into purple product and gradually turns black after light exposure. With the application of antibacterial agents, the color may affect the derivative products and restrict the
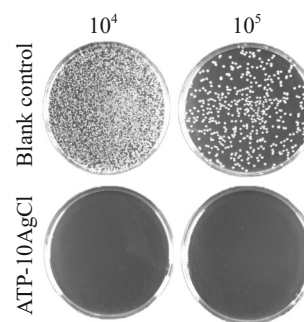
Fig.7 MIC test results of E. coli with ATP-10AgCl composite and blank control group at dilution ratios of 10^4 and 10^5
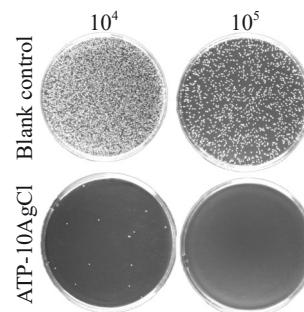
Fig.8 MIC test results of S. aureus with ATP-10AgCl composite and blank control group at dilution ratios of 10^4 and 10^5
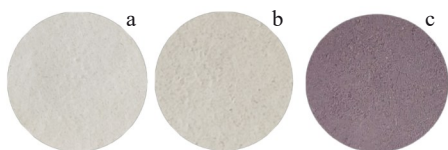
Fig.9　Appearances of ATP (a), ATP-10AgCl composite (b), and AgCl (c) after light exposure for 24 h

Fig.10　Schematic diagrams of antibacterial mechanisms of ATP-AgCl composites

practical application to a certain extent. However, the composites remain offwhite even after light exposure for 24 h.

2.4　Antibacterial mechanism of ATP-AgCl composites

Two possible mechanisms are proposed. One theory is that the large-size AgCl NPs accumulate on the cell wall to denature the cell initially; then, the AgCl NPs with the size less than 10 nm directly penetrate the cell membrane to destroy the bacteria (Fig. 10)[27–28]. The other theory is related to the antibacterial effect of Ag^+. A small amount of Ag^+ dissolves from the composites and penetrates the cell wall[29]. Some Ag^+ ions loaded on the cell membrane destroy the metabolism of membrane; others enter the cell and react with the functional groups containing sulfur and ammonia in proteins[30] and nucleic acids[31], causing protein coagulation, destroying the activity of cell synthase, and leading to the death of bacteria. After the inactivation of bacteria, Ag^+ and small-size AgCl NPs are separated from the bacteria and sterilized repeatedly for the lasting antibacterial effect[32–33].

3　Conclusions

1) ATP-AgCl composites can be prepared by simple and flexible hydrothermal method with ATP as carrier.

2) The introduction of ATP avoids the agglomeration of AgCl NPs and reduces the particle size from 5–10 μm to 3–20 nm. The as-prepared composites exhibit excellent photostability: the color changes slightly even after light exposure for 24 h.

3) The composites exhibit excellent antibacterial activity. With the small loading of 10wt% AgCl, the diameters of inhibition circles against E. coli and S. aureus are 6 and 8 mm, respectively. This result indicates that the ATP-10AgCl composite has comparable antibacterial effect as pure AgCl, which is beneficial to reduce the manufacture cost. The antibacterial ratios against E. coli and S. aureus are 99.98% and 99.88%, respectively.

References

1　Li Yuan, Han Lingjue, Wang Yue *et al*. *Materials China*[J], 2023, 42(2): 144 (in Chinese)

2　Zhang Zhongbo, Li Xiuqin, Li Boxuan *et al*. *Rare Metal Materials and Engineering*[J], 2022, 51(3): 1017 (in Chinese)

3　Kong Wenquan, Wei Kai, Zhao Yao *et al*. *Rare Metal Materials and Engineering*[J], 2023, 52(7): 2623 (in Chinese)

4　Chen Hong, Ren Yuyu, Ding Jian *et al*. *Rare Metal Materials and Engineering*[J], 2023, 52(2): 745 (in Chinese)

5　Cartwright A, Jackson K, Morgan C *et al*. *Agronomy-Basel*[J], 2020, 10(7): 1018

6　Toan L V, Thong N H, Quan D H *et al*. *J Appl Spectrosc*[J], 2022, 89(3): 482

7　Yu, Z Y, Liu Y Q, He W *et al*. *Catal Today*[J], 2019, 335: 574

8　Fanoro O T, Oluwafemi O S. *Pharmaceutics*[J], 2020, 12(11): 1044

9　Al-Tayyar N A, Youssef A M, Al-Hindi R R. *Food Packaging Shelf*[J], 2020, 25: 100523

10　Mei L, Zhu S, Yin W *et al*. *Theranostics*[J], 2020, 10(2): 757

11　Mohapatra B, Mohapatra S, Sharma N. *Ceram Int*[J], 2023, 49(12): 20218

12　Wang Wenbo, Mu Bin, Zhang Junping *et al*. *Scientia Sinica Chimica*[J], 2018, 48(12): 1432 (in Chinese)

13　Zhao P, Liu Y H, Liu B *et al*. *Materials Express*[J], 2022, 12(1): 166

14　Liu X Q, Duan X C, Yan R F *et al*. *J Mater Civil Eng*[J], 2008, 10: 173

15　Shi W X, Duan Y S, Yi X S *et al*. *Desalination*[J], 2013, 317: 41

16　Li X Z, He C L, Zuo S X *et al*. *Sol Energy*[J], 2019, 191: 251

17　Zhang C T, Hu X, Yu Z J *et al*. *Int J Hydrogen Energ*[J], 2019, 44(11): 5230

18　Zhao D, Zhou J, Liu N. *Bulletin of the Chinese Ceramic Society*[J], 2005, 24(3): 67

19　Chernousova S, Epple M. *Angew Chem Int Edit*[J], 2013, 52(6): 1636

20　Kumar D A, Palanichamy V, Roopan S M *et al*. *J Photoch Photobio B*[J], 2014, 138: 302

21　Choi O, Deng K K, Kim N J *et al*. *Water Res*[J], 2008, 42(12): 3066

22　Mao C Y, Xiang Y M, Liu X M *et al*. *Acs Nano*[J], 2017, 11(9): 9010

23　Godoy-Gallardo M, Eckhard U, Delgado L M *et al*. *Bioact Mater*[J], 2021, 6(12): 4470

24　Yin I X, Zhang J, Zhao I S *et al*. *Int J Nanomed*[J], 2020, 15: 2555

25　Chauhan A, Chauhan P. *J Anal Bioanal Tech*[J], 2014, 5(5): 1000212

26　Liao C, Li Y, Tjong S C. *Int J Mol Sci*[J], 2019, 20(2): 449

27 Asharani P V, Hande M P, Valiyaveettil S. *Bmc Cell Biol*[J], 2009, 10: 65

28 Ahmed K B R, Nagy A M, Brown R P *et al. Toxicol In Vitro*[J], 2017, 38: 179

29 Rieger K A, Cho H J, Yeung H F *et al. Interfaces*[J], 2016, 8(5): 3032

30 Mijnendonckx K, Leys N, Mahillon J *et al. Biometals*[J], 2013, 26(4): 609

31 Kedziora A, Speruda M, Krzyzewska E *et al. Int J Mol Sci*[J], 2018, 19(2): 444

32 Morones-Ramirez J R, Winkler J A, Spina C S *et al. Sci Transl Med*[J], 2013, 5(190): 190ra81

33 Gordon O, Slenters T N V, Brunetto P S *et al. Chemotherapy*[J], 2010, 54(10): 4208

原位合成高效抗菌活性凹凸棒石负载氯化银纳米粒子复合材料

张可风[1,2]，李　艳[1,2]，乜开龙[1,2]，党诗源[1,2]，药秉学[1]，滑　雪[1,2]，田光燕[1,2]

(1. 河北工业大学 材料科学与工程学院，天津 300130)

(2. 河北工业大学 生态环境与信息特种功能材料教育部重点实验室，天津 300130)

摘　要： 为提高AgCl纳米粒子（NPs）的分散性和光稳定性，将AgCl NPs锚定在凹凸棒石（ATP）表面制备了ATP-AgCl复合材料，研究了其微观形貌、晶体结构及抗菌性能。结果表明：ATP的引入有效避免了AgCl NPs的团聚，AgCl NPs的粒径从5~10 µm显著减小到3~20 nm。由于纳米粒子的小尺寸效应，ATP-AgCl复合材料表现出与纯AgCl相媲美的抗菌活性，其对大肠杆菌和金黄色葡萄球菌的抗菌率分别达到99.98%和99.88%。此外，ATP的引入还显著改善了AgCl NPs的光稳定性，复合材料经24 h阳光暴晒后仍保持原始的灰白色。

关键词： 凹凸棒石；氯化银；无机抗菌剂；大肠杆菌；金黄色葡萄球菌